

## EVALUATION OF SECONDARY FAULT ACTIVITY USING LOCAL SAFETY FACTOR OF ROCK MASS COMPUTED BY PARALLEL FNITE ELEMENT METHOD

**Kazumoto Haba<sup>1</sup>, Masataka Sawada<sup>2</sup>, Kazuaki Watanabe<sup>3</sup>, and Muneo Hori<sup>4</sup>**

<sup>1</sup>Manager, Taisei Corporation, Tokyo, Japan (hb-kzm00@pub.taisei.co.jp)

<sup>2</sup>Senior Research Scientist, Nuclear Risk Research Center, Central Research Institute of Electric Power Industry, Chiba, Japan

<sup>3</sup>Acting General Manager, Taisei Corporation, Tokyo, Japan

<sup>4</sup>Principal Scientist, Japan Agency for Marine-Earth Science and Technology, Kanagawa, Japan

### ABSTRACT

In Japan, assessment of secondary faults is required for the safety of Nuclear Power Plants (NPPs). From the viewpoint of mechanics, the secondary fault activity can be estimated by analysing a high-fidelity rock mass model. In this paper, we present a parallel finite element method for such a model. We demonstrate the assessment of the secondary fault using this numerical analysis method, reproducing an actual earthquake that includes secondary faults.

### INTRODUCTION

In the 2023 Turkey-Syria earthquake, surface earthquake faults appeared over a wide area and damaged structures. In Japan, earthquakes with surface faults have also occurred in recent years, such as the 2014 Nagano-ken Hokubu earthquake and the 2016 Kumamoto earthquake. For the safety of NPPs in Japan, assessment of secondary faults is required.

The key issue on the secondary fault assessment is to consider the location of surface faults induced by the secondary fault. The location of the surface fault induced by the primary fault, can be estimated from aerial photographs and literature surveys; see Figure 1. However, it is difficult to estimate the location of the surface fault induced by the secondary faults since the secondary fault activity is infrequent and the surface faults are of small size. Secondary faults are formed in association with the activity of the primary fault although they have no geotectonic association with the earthquake source fault, as shown in Figure 1. Therefore, the best estimate for the location of the surface fault induced by the secondary faults is made by accurately estimating the stress of the near-surface rock mass during earthquakes.

Stress of the rock mass during earthquakes can be calculated by kinematic ground motion analysis. A parallel FEM, which implements a conjugate gradient matrix solver for high scalability, is needed to accurately calculate the stress using a high-fidelity rock mass model. E-FrontISTR (Motoyama et al., 2021) was used as such a parallel FEM. It was developed by Taisei Corporation, Central Research Institute of Electric Power Industry, The University of Tokyo, Tokyo Electric Power Services CO., National Research Institute for Earth Science and Disaster Resilience, and Ark Information Systems. In this paper, we present a method for estimating the occurrence areas of secondary faults based on the stress of the rock mass which computed by kinematic ground motion analysis using a parallel FEM. We focus on the local safety factor (LSF) for the assessment of the secondary fault activity (Haba et al. (2023)). The LSF is defined by the ratio of shear stress to strength and is practically used as an index to evaluate the possibility of fracture propagation in seismic stability assessment of slope/foundation for NPPs in Japan.

The remainder of this paper is organised as follows. First, explained is the method of secondary fault estimate using the parallel FEM that analyses the stress of the rock mass during an

earthquake. A ground motion analysis is performed for an actual earthquake, and the location of secondary faults is estimated using the LSF based on the stress of the rock mass. Discussions are made on the results obtained for the numerical analysis.

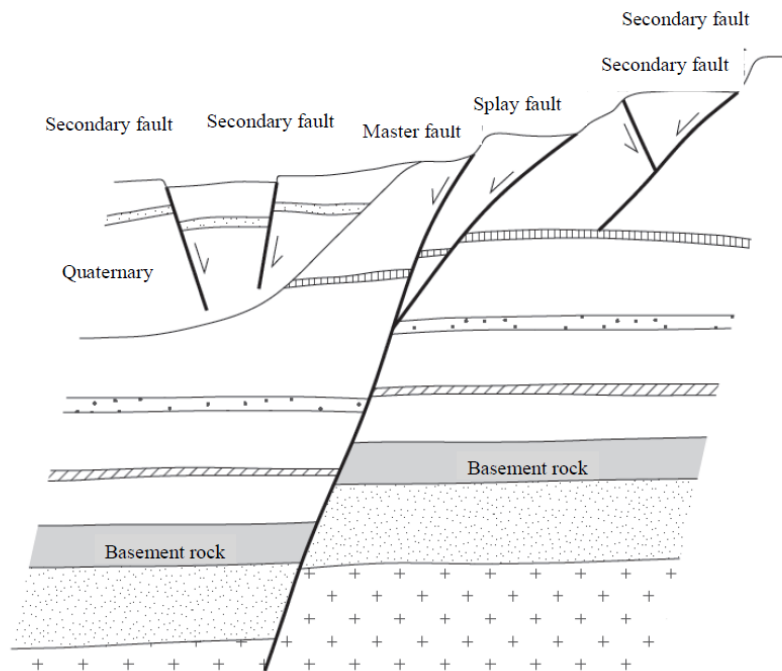


Figure 1. Classification of Surface Earthquake Faults by Japan Nuclear Safety Institute (2013).

## METHOD

The seismic stress of the rock mass is the sum of the stress generated by the ground motion analysis and the stress computed for the gravity analysis that estimates the initial stress state.

The former stress is computed by the kinematic ground motion analysis that uses the parallel FEM. High-fidelity ground models which include the ground surface and subsurface structure are used in this analysis. The J-SHIS deep geological model data and the Japan National Primary Subsurface Model are used to determine the surface and subsurface structure. The finite element mesh is generated using the octree method based on a procedure as shown in Figure 2. Strata boundaries become staircase shapes, while the ground surface becomes a smooth shape. The smooth configuration of the ground surface is important for estimating the stress in the rock mass near the ground surface.

In the kinematic ground motion analysis, a slip on a fault plane is replaced by an equivalent double-couple force. Thus, an earthquake source slip is replaced by a set of point-wise double-couple forces. The density of the point-wise double-couple forces significantly affects the stress distribution in the vicinity of the source fault. Instead of the point-wise double-couple forces, we use a distributed double-couple forces proposed by Habu *et al.*, 2023; the equivalent double-couple forces are smoothly distributed on the earthquake fault plane. The distributed double-couple force results in much higher accurate estimate of stress the vicinity of the earthquake source fault. This accurate estimate is essential for the estimate of the secondary fault activity.

We used the LSF defined in Figure 2 to evaluate the occurrence of a surface fault induced by the secondary faults (Habu *et al.* (2023)). The kinematic ground motion analysis uses the LSF to estimate the initiation point of rupture. More specifically, the LSF in the shallow part of the rock mass is computed during the process of the earthquake and the occurrence of surface faults induced by the secondary faults is evaluated based on the time series of the computed LSF.

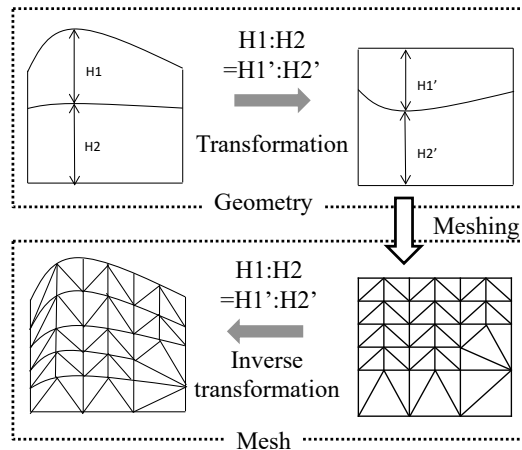


Figure 2. Procedure for generating a finite element mesh with a smooth shape of the ground surface. The geometry of ground was transformed into a rectangular shape while maintaining the layer thickness ratio of each layer. After meshing, the mesh is inverse transformed.

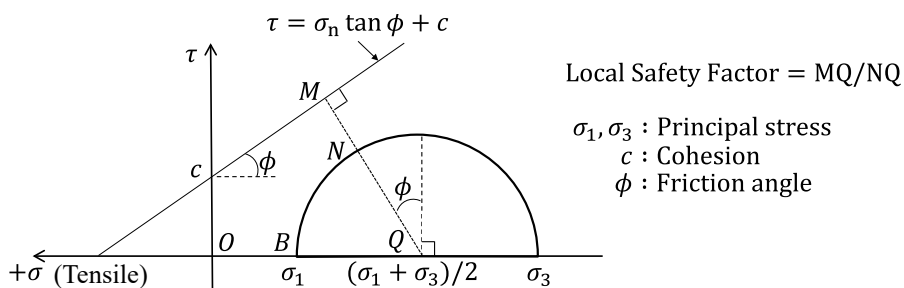


Figure 3. Local safety factor

## GROUND MOTION ANALYSIS FOR AN ACTUAL EARTHQUAKE

In this section, we present a ground motion analysis for the 2014 Nagano-ken Hokubu earthquake using parallel FEM (Haba et al. (2023)).

### *The 2014 Nagano-ken Hokubu earthquake*

We conducted a ground motion analysis for the 2014 Nagano-ken Hokubu earthquake, which occurred on 22 November 2014 and had a JMA magnitude of 6.7. The earthquake was a reverse fault earthquake with a west-northwest-east-southeast compressional axis and relative uplift to the east side. A 9-km long surface rupture was observed on the Kamishiro fault. In addition, surface faults induced by secondary faults were observed at the northern end of the primary surface fault, as shown in Figure 3. Here the secondary faults b2 and b3 which appeared parallel to the primary fault are back-thrust faults.

The spatially and temporally changing slip distribution on the earthquake source fault were obtained from a seismic source inversion analysis performed by Hikima et al. (2015). The strike angle, dip angle, length and width of the source fault were 25° and 50° 19.5 km and 15 km, respectively. The final slip distribution and the norm of the slip velocity time function are shown in Figure 4. They are computed for each 1.5 km × 1.5 km square segment. The rupture propagation velocity was 2.0 km/s in the two shallow parts from the top and 2.8 km/s in the deeper part. The shear modulus of the rock mass was 3.0 × 10<sup>7</sup> kPa.

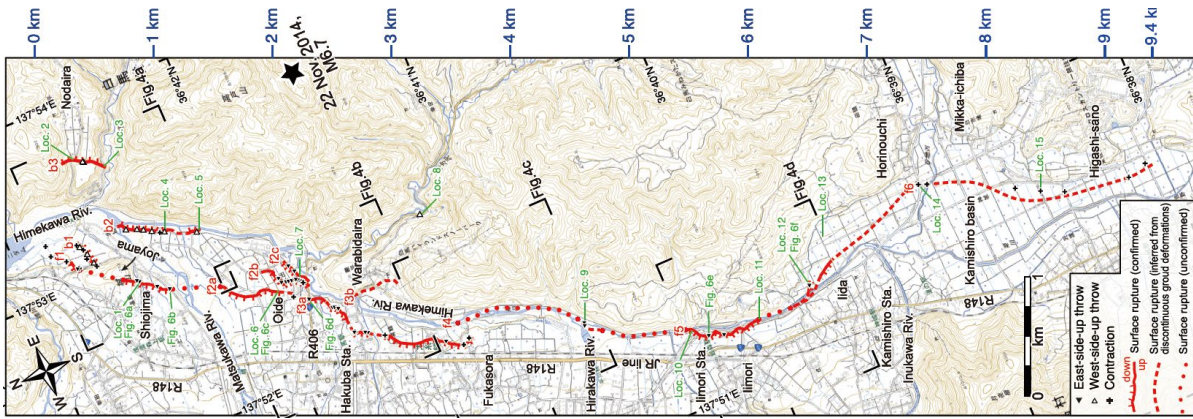


Figure 4. Distribution of surface faults of the 2014 Nagano-ken Hokubu earthquake (Ishimura et al. (2015)).

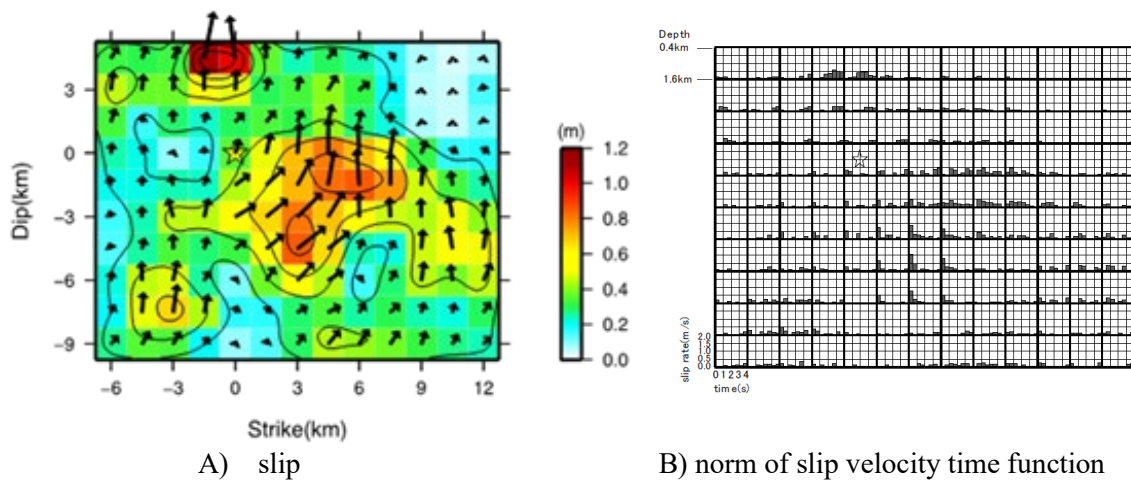


Figure 5. Slip distribution on the earthquake source fault derived by Hikima et al. (2015).

**Analysis model and calculation condition**

Figure 5 shows a high-fidelity analysis model with a size of 40 km × 40 km × depth of 20 km, including the entire area of the earthquake source fault described as a white line. The +y direction corresponds to the north. The geometry of ground surface and subsurface structure was determined based on the J-SHIS deep geological model data and the Japan National Primary Subsurface Model. The seven geological layers listed in Table 1 are modelled. Second-order tetrahedral solid elements were used. The target frequency is set to 2.5 Hz, and the minimum element size is set to 31.25 m. The total number of degrees of freedom is 228,465,240. Viscous boundaries were set at the side and bottom boundaries of the analysis model for ground motion analysis. The rock mass was assumed a linearly elastic body and Table 1 summarizes the material properties. Rayleigh damping was used and the damping constants were set to satisfy the damping ratio which was derived from the Q values at 0.1 Hz and 4.0 Hz.

The source model derived by Hikima et al (2015) is used as a plane source for the kinematic fault model. The shear modulus of the second to the fifth layers used to calculate the double couple force was set at  $1.5 \times 10^7$  kPa, considering the average value of the shear modulus of the rock mass. The failure initiation time was determined by dividing each 1.5 km × 1.5 km segment into 10 sections. The analysis is performed up to 20 seconds with 0.01 second increments.

In the initial stress analysis, the side and bottom boundaries of the analysis model were fixed in the normal direction, and the gravity acceleration was applied. Young's modulus of the four shallow layers was unified with the value of the fourth layer. Poisson's ratio was set to 0.49.

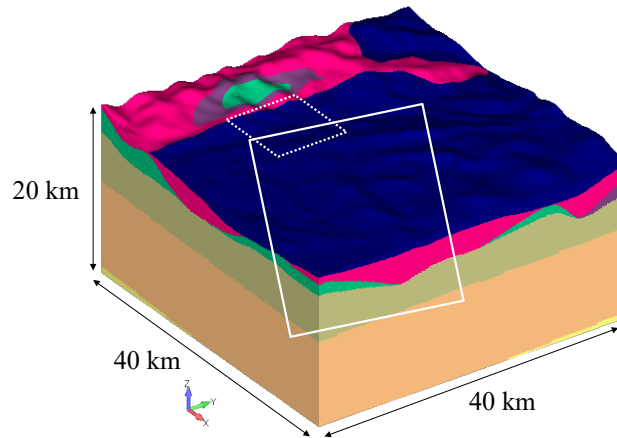


Figure 6. Analysis model. The white, and white dotted lines indicate the position of the Kamishiro fault, and an area of observed surface faults, respectively.

Table 1. Material properties of the rock mass

No	<i>P</i> -wave velocity (m/s)	<i>S</i> -wave velocity (m/s)	Density (kg/m <sup>3</sup> )	Q Value
1	2500	1000	2100	150
2	3800	2000	2400	200
3	4000	2100	2400	300
4	5000	2700	2500	200
5	5500	3100	2600	300
6	5800	3400	2700	680,400
7	6400	3800	2800	680,400

### ***Results of displacement***

The distribution of the vertical displacement components (in the *z*-direction) on the ground surface at the last step is shown in Figure 6; A) for the entire calculation area and B) for the area where the surface faults were observed, indicated by the black dotted square in A). The black dotted and solid lines in Figure 6 B) are the observed surface faults induced by the primary and secondary faults, respectively. The vertical displacement distribution corresponds to a reverse fault type with uplift on the east side.

The calculated displacements at the electronic reference point Hakuba (950266) are 0.20 m eastward, 0.14 m southward, and a subsidence of 0.13 m, which are in good agreement with the observed results of 0.26 m eastward, 0.14 m southward, and a subsidence of 0.12 m. Figure 7 shows the time series of the displacement at the station NGNH36 of the KiK-net, a strong-motion network operated by the National Research Institute for Earth Science and Disaster Prevention (NIED). The red and black lines are the computed results and the observed records, respectively. It is seen that the numerical analysis reproduces the observed record satisfactorily.

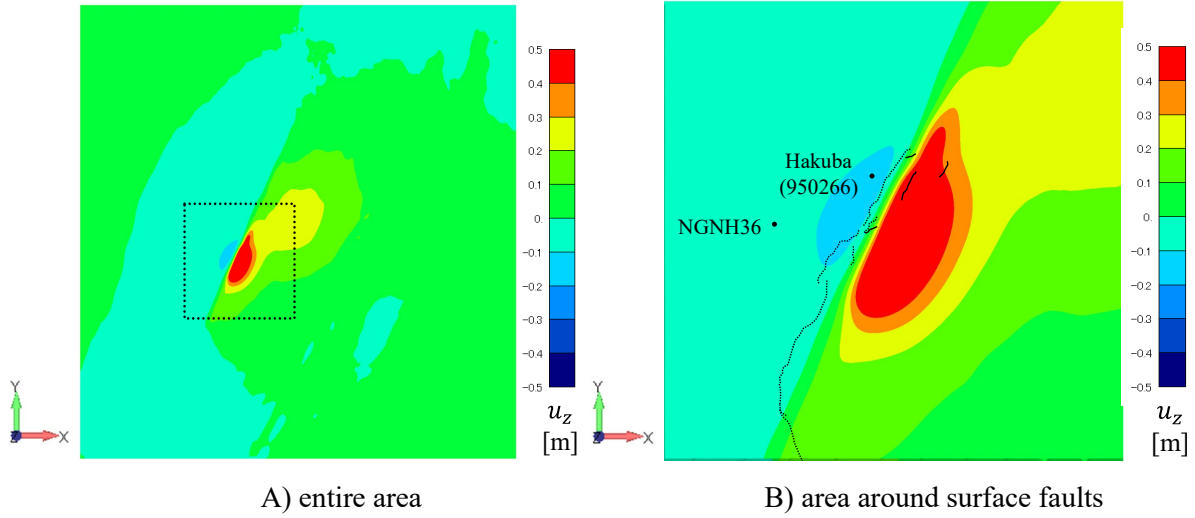


Figure 7. Displacement of up and down direction on ground surface. In B), black dotted and black lines are the observed primary faults and secondary faults, respectively. Black dots are the station NGNH36 of the KiK-net and the electronic reference point Hakuba (950266).

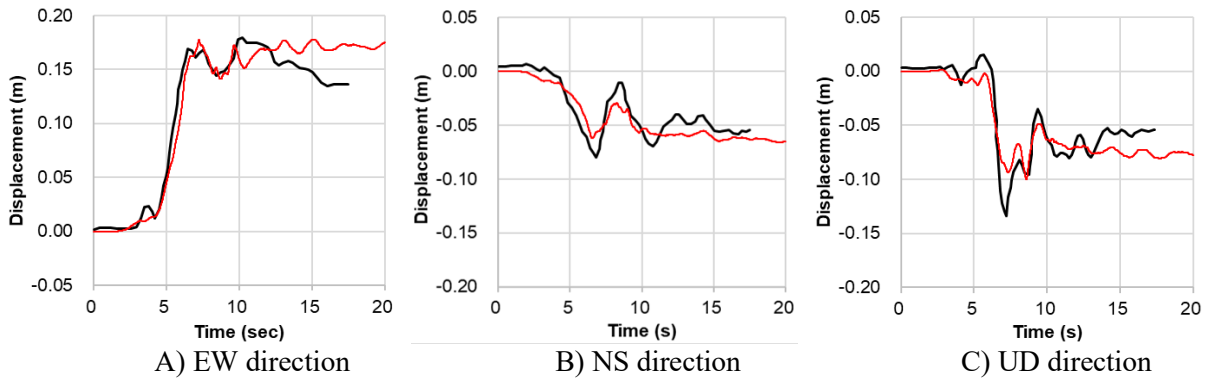


Figure 8. Time histories of displacements at the station NGNH36 of the KiK-net. The red and black lines are numerical results and observations, respectively.

### ESTIMATION OF SECONDARY FAULTS BASED ON ROCK MASS STRESS

In this section, we demonstrate an estimation of the secondary fault activity based on the LSF (Haba et al. (2023)). Since there is no information on the strength of the rock mass, that is characterized in the two material parameters, namely, the cohesion  $c$  and the internal friction angle  $\phi$ , we consider two sets of  $c$  and  $\phi$ ; the first set is  $c = 1.2$  MPa and  $\phi = 30^\circ$ , and the second set is  $c = 0.9$  MPa and  $\phi = 25^\circ$ . The LSFs at the last step around the observed surface faults are shown in Figure 8, where the observed surface faults are given by black lines; A) for the first set and B) for the second set. In Figure 8 A), there are two zones with LSFs  $< 1$ . The zone on the  $-x$  side is consistent with the observation of the primary fault, and the zone on the  $+x$  side coincides with the secondary fault b2. In addition, an area of a relatively low LSF is found at a distance of about 1 km from the primary fault, corresponding to the secondary fault b3, although the LSF is not less than 1. In Figure 6 B), it is seen that the LSF at the location of the secondary fault b3 is less than 1 in the second set, i.e.,  $c = 0.9$  MPa and  $\phi = 25^\circ$ . These results suggest that the secondary faults occur in the region of  $LSF < 1$ . We note that surface faults do not always occur in the region of small LSF, but they do occur somewhere with small LSF.

Figure 9 shows the NQ and the MQ, where  $LSF = MQ/NQ$ , at the last step around the observed surface faults. NQ is the maximum principal shear stress, MQ is related to the shear strength

which depends on the confining pressure. Figure 9 A) shows that two zones of relatively larger NQ appear on the ground surface. They correspond to the primary fault and a secondary fault b2 by comparison with the observed surface faults. Figure 9 B) shows the MQ in the case of  $c = 1.2$  MPa and  $\phi = 30^\circ$ . The MQ is large in the region corresponding to the primary fault and small in the region corresponding to the secondary fault. This is because the region of the primary fault is in compression, whereas one of the secondary faults is closer to tension. These results indicate that the LSF, which is a function of both stress and strength, is suitable for estimating the areas where secondary faults can occur, since the strength changes significantly with the confining pressure during earthquakes with the fling step.

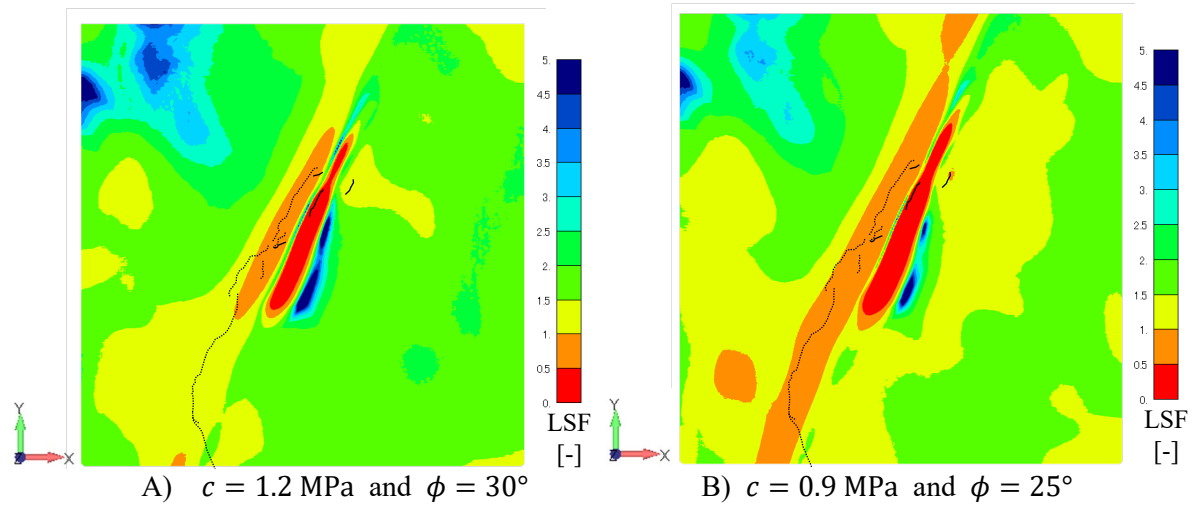


Figure 9. Local safety factor on ground surface around the observed secondary faults.

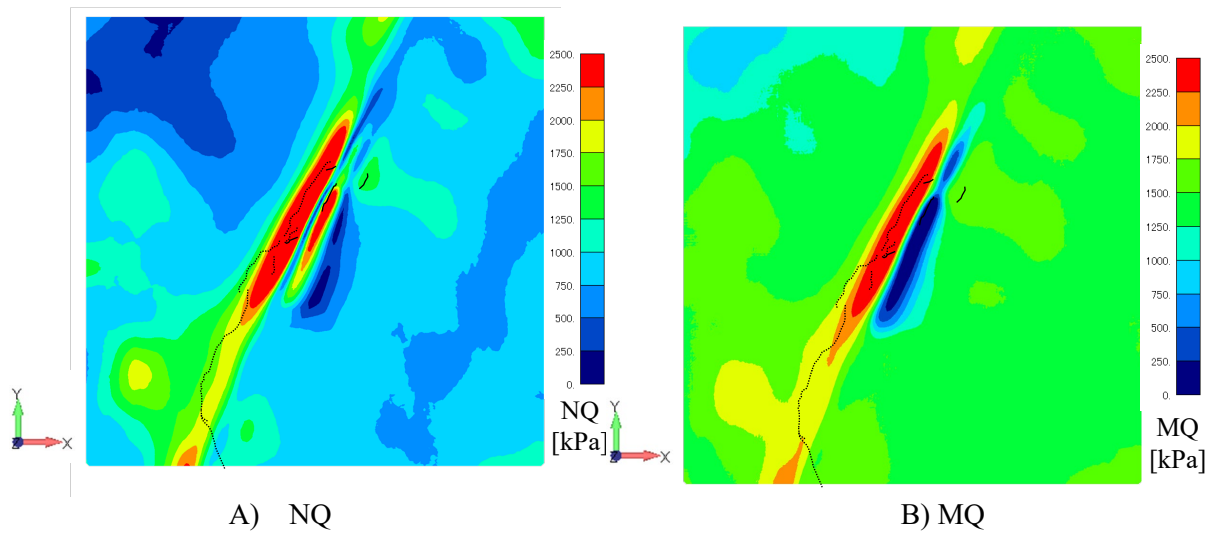


Figure 10. NQ and MQ on ground surface around the observed secondary faults. MQ is the result in the case of  $c = 1.2$  MPa and  $\phi = 30^\circ$ .

## CONCLUSION

In this paper, we evaluated the stress of the rock mass by ground motion seismic analysis using a parallel FEM and estimated the locations of surface secondary faults based on the LSF. As a result, several zones of low LSF were found on the ground surface, which were in good agreement with the observed surface faults. These results suggest that the LSF can be used to estimate where the secondary fault may occur. It should be noted that fault rupture may not necessarily occur throughout the entire low LSF area, but rupture can start somewhere in the low area because the ground motion analysis is a linear elastic analysis that does not consider the propagation of rupture. Therefore, if the LSF in the target area is low, we should evaluate the occurrence of secondary faults more precisely. In this case, it is necessary to perform a numerical analysis that takes into account the rupture of the fault plane.

## ACKNOWLEDGEMENT

The analyses in this paper were partly performed using the Earth Simulator of the Japan Agency for Marine-Earth Science and Technology. The J-SHIS deep ground database of the NIED was used for the analyses. Waveform records from K-NET and KiK-net of the NIED were used. Dr. K. Hikima of Tokyo Electric Power Company, Inc. provided the source inversion results. We would like to express our gratitude for their cooperation.

## REFERENCES

- Haba, K., Sawada, M., Watanabe, K., and Hori, M. (2023), Finite element analysis of round motion using plane source and estimation of occurrence region of secondary faults based on stress of rock mass, *Japanese Journal of JSCE*, 79(13), 22-13035. (in Japanese)
- Headquarters for Earthquake Research Promotion, Japanese integrated velocity structure model, long-period ground motion hazard map 2012, [http://www.jishin.go.jp/main/chousa/12\\_choshuki/choshuki2012\\_a2.pdf](http://www.jishin.go.jp/main/chousa/12_choshuki/choshuki2012_a2.pdf) (Accessed on October 30, 2023.)
- Ishimura, D., Okada, S., Niwa, Y. and Toda, S. (2015). The surface rupture of the 22 November 2014 Nagano-ken-hokubu earthquake (Mw 6.2), along the Kamishiro fault, Japan, *Active Fault Research*, 2015, 43: 95-108.
- Japan Nuclear Safety Institute (2013). Assessment methods for nuclear power plant against fault displacement.
- Motoyama, H., Sawada, M., Hotta, W., Haba, K., Otsuka, Y., Akiba, H. and Hori, M. (2021). Development of a general-purpose parallel finite element for analyzing earthquake engineering problems, *Earthq. Engng, Struct. Dyn.*, 50: 4180-4198.
- National Research Institute for Earth Science and Disaster Resilience, J-SHIS Japan Seismic Hazard Information Station, <http://www.j-shis.bosai.go.jp/> (Accessed on October 30, 2023)